molecular pharmaceutics

ARTICLE

pubs.acs.org/molecularpharmaceutics

^{18}F-Labeled Modified Porous Silicon Particles for Investigation of Drug Delivery Carrier Distribution in Vivo with Positron Emission Tomography

Mirkka Sarparanta,[*,†] Ermei Mäkilä,[‡] Teemu Heikkilä,[‡] Jarno Salonen,[‡] Edwin Kukk,[§] Vesa-Pekka Lehto,[∥] Hélder A. Santos,[⊥] Jouni Hirvonen,[⊥] and Anu J. Airaksinen[†]

[†]Laboratory of Radiochemistry, Department of Chemistry, University of Helsinki, FI-00014 University of Helsinki, Finland

[‡]Laboratory of Industrial Physics, Department of Physics and Astronomy, University of Turku, FI-20014 University of Turku, Finland

[§]Materials Research Laboratory, Department of Physics and Astronomy, University of Turku, FI-20014 University of Turku, Finland

[∥]Department of Applied Physics, University of Eastern Finland, FI-70211 Kuopio, Finland

[⊥]Division of Pharmaceutical Technology, Faculty of Pharmacy, University of Helsinki, FI-00014 University of Helsinki, Finland

Supporting Information

ABSTRACT: Because of its biocompatibility and ability to accommodate a variety of payloads from poorly soluble drugs to biomolecules, porous silicon (PSi) is a lucrative material for the development of carriers for particle-mediated drug delivery. We report a successful direct one-step ^{18}F-radiolabeling of three types of PSi microparticles, thermally hydrocarbonized THCPSi, thermally oxidized TOPSi, and thermally carbonized TCPSi for the investigation of their biodistribution in vivo with positron emission tomography as part of their evaluation as carriers for particle-mediated drug delivery. FTIR and XPS characterization of the PSi materials after carrier-added ^{18}F/^{19}F-radiolabeling reveals that depending on the material the ^{18}F-labeling is likely to be accomplished either by substitution for surface silyl hydrogen or silyl fluoride or by nucleophilic attack of $^{18}F^-$ to Si−O−Si bridges. With the selected ^{18}F-radiolabeling method, good to excellent in vitro radiolabel stability in simulated gastric and intestinal fluids and in plasma is achieved for all the particle types studied. Finally, a preliminary evaluation of ^{18}F-THCPSi microparticle biodistribution in the rat gastrointestinal tract after oral administration is reported, illustrating the utility of using ^{18}F-radiolabeled PSi as imaging probes for PSi-based drug delivery carrier distribution in vivo.

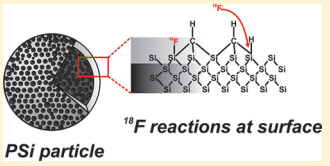

KEYWORDS: drug delivery, fluorine-18, porous silicon, positron emission tomography (PET)

1. INTRODUCTION

Molecular imaging methods, such as positron emission tomography (PET), can greatly facilitate the development of novel carriers for particle-mediated drug delivery, as they can be employed in essentially all the steps of targeted delivery system evaluation: from carrier material in vivo characterization to target validation and evaluation of drug target engagement.[1,2] Porous silicon materials are a promising platform for the design of novel nano- and microscaled devices for targeted drug delivery and controlled drug release. Successful loading into and release from PSi particles has been shown in vitro for several drugs and biomolecules[3−8] and magnetic and fluorescent secondary nanoparticle payloads.[9,10] In vivo, successful delivery of therapeutic peptides,[11] siRNA[12] and anticancer agent doxorubicin[13] has been reported. Improved dissolution of poorly soluble drugs and favorable release kinetics after loading into PSi microparticles have been demonstrated, rendering the approach a promising option to increase drug bioavailability after oral administration.[7]

PSi is predominantly produced by electrochemical etching with hydrofluoric acid, where material porosity, pore diameter and volume can be controlled by the etching conditions. As all of these are important factors for loading and delivery of the payload as well as material biocompatibility, the possibility to fine control these sets PSi apart from most other materials currently in use for particle-mediated drug delivery.[4,14,15] The freshly prepared hydrogen-terminated PSi surface easily oxidizes at ambient air and is therefore usually removed or replaced using thermal or chemical treatment. Common surface modifications include oxidation, hydrosilylation and thermal carbonization. Additionally, the particles can be coated with polymers or biomolecules in order to prolong circulation time by masking them from the uptake by the reticuloendothelial system (RES), the main obstacle in systemic particle-mediated drug delivery.[9,13,16]

A unique feature of PSi is its biocompatibility, specifically the effect of porosity and pore size thereupon.[17] Several studies have confirmed the biocompatibility of PSi implants in the eye and particles after acute intravenous and subcutaneous administration.[11,18,19] PSi is

Received: April 1, 2011
Accepted: August 29, 2011
Revised: August 11, 2011
Published: August 29, 2011

ACS Publications © 2011 American Chemical Society

dx.doi.org/10.1021/mp2001654 | *Mol. Pharmaceutics* 2011, 8, 1799–1806

largely deemed biodegradable with the main degradation product being orthosilicic acid that is excreted in urine. Biodegradability and the rate of degradation can be affected greatly by the porosity, pore size distribution and surface chemistry of the material.[8,20,21] The cytotoxicity and cellular association of PSi particles have been intensively studied in vitro. Recent reports have shown a dependence of cytotoxic effects including reduced cell viability and intracellular ROS and TNF-α production of particle size and surface chemistry.[22,23]

Many porous silicon materials exhibit intrinsic luminescence that conveniently allows for their direct detection in cell preparations, in excised organs and in vivo in small laboratory animals.[13,24,25] Therefore, primarily luminescence and fluorescence imaging methods have been employed in in vivo and in vitro studies of PSi particle biodistribution, biocompatibility, elimination and cellular association.[9,13,22,23,26] However, the development of nuclear imaging methods such as PET to study PSi behavior in vivo is necessitated by the limited quantitativeness and translationality of the above-mentioned imaging modalities from laboratory rodents to humans. Fluorine-18 is a short-lived positron emitter used in a plethora of radiopharmaceuticals for PET because of its favorable imaging properties and the possibility for multistep syntheses and transport of the finished tracer allowed by the 109.8 min half-life of the isotope. Additionally, the high specific radioactivity of cyclotron-produced ^{18}F (typically around 185 GBq μmol^{-1}) enables the use of a tracer amount of the isotope in the labeling reaction resulting in often negligible change in particle properties and, consequently, in vivo behavior.[22,27]

The high bond energy of the silicon−fluoride bond has made the use of Si−^{18}F labeling synthons a lucrative synthetic approach in ^{18}F-radiochemistry, because, due to the high affinity of fluorine to silicon, a silyl hydrogen can be readily replaced by ^{18}F$^-$. Different ^{18}F-fluorosilane prosthetic groups have been successfully employed for facile one-step radiolabeling of peptides under mild conditions with organoethoxysilane and ^{18}F-di-*tert*-butylphenylfluorosilane precursors.[28−32] Interestingly, ^{18}F-radiolabeling methods have been recently developed for lanthanide nanoparticles[33,34] as well as nanodiamonds.[35] Here, we have employed a direct synthetic strategy to introduce the ^{18}F label on the PSi surface by substitution of ^{18}F for oxygen in Si−O−Si bridges and possible residual silyl hydrogens on the surface. The studied surface modifications of PSi were thermal hydrocarbonization (THCPSi, Si−C−H$_x$), thermal oxidation (TOPSi, Si−O$_x$), and thermal carbonization (TCPSi, Si−C$_x$). Carrier-added ^{18}F-radiolabeling of PSi particles and free-standing films was used to investigate the incorporation of fluorine to the materials in the radiolabeling reaction. Radiolabel stability was determined in buffer solutions at physiological pH range, in simulated gastric and intestinal fluids and in human plasma, and finally a biodistribution study with orally administered ^{18}F-THCPSi microparticles was carried out in rats to demonstrate the feasibility of using ^{18}F-radiolabeling to follow the passage of the particles in the gastrointestinal (GI) tract.

2. MATERIALS AND METHODS

2.1. Fabrication of PSi Microparticles. The preparation and characterization of PSi microparticles has been described in detail previously.[3,8,22,36] Briefly, free-standing PSi films were fabricated by electrochemically anodizing monocrystalline Si(100) wafers in a 1:1 (v/v) hydrofluoric acid (38%)−ethanol solution with a constant current density of 50 mA cm^{-2}. The silicon wafers were p+-type, boron-doped with a resistivity of 0.01−0.02 Ω cm. The porosified layer was separated from the wafer by abruptly increasing the etching current to the electropolishing region. Microparticles were prepared by milling the PSi films with a high energy ball mill (Pulverisette 7, Fritsch GmbH) in an agate grinding jar. The particles were dry and wet sieved in ethanol in order to obtain the desired size fraction of 1−38 μm or 1−10 μm, for radiolabeling synthesis development and biodistribution studies, respectively. Thermally oxidized PSi (TOPSi) was prepared by placing the particles into a furnace at 300 °C for two hours in ambient air. Prior to the thermal carbonization or hydrocarbonization treatments the PSi films and microparticles were immersed into HF−ethanol solution to remove the natural oxide layer and refresh the surface hydride species. After the immersion the PSi were dried at 65 °C for several hours. Thermally hydrocarbonized PSi (THCPSi) were prepared as described earlier,[36] with 15 min treatment at 500 °C under constant N_2:acetylene flush. Thermally carbonized PSi (TCPSi) was prepared by using a two-step carbonization method described in detail by Salonen et al.[3] The initial step in the treatment is as for the thermal hydrocarbonization, followed by additional treatment at 820 °C under N_2 flush for 10 min.

Table 1. Characterization Data of the PSi Microparticles

material	specific surface area[a] ($m^2\ g^{-1}$)	pore vol[a] ($cm^3\ g^{-1}$)	av pore diam[a] (nm)
THCPSi	311	1.036	13.0
TCPSi	262	1.099	16.8
TOPSi	260	1.100	16.3

[a] Characterization data calculated from the desorption branch of the nitrogen sorption isotherm using the BJH theory.

The properties of the PSi microparticles were characterized with nitrogen sorption at 77 K using TriStar 3000 gas sorption apparatus (Micromeritics Inc.). The specific surface area, pore volume and average pore diameter were calculated from the desorption branch of the measured isotherm using Barrett−Joyner−Halenda (BJH) theory. Characterization data for the particles is given in Table 1.

2.2. ^{18}F-Radiolabeling of the Microparticles. ^{18}F was produced on an IBA Cyclone 10/5 cyclotron in an ^{18}O(p,n)^{18}F reaction. ^{18}F$^-$ was trapped in an anion exchange cartridge (Waters Sep-Pak QMA Light Plus, Waters Corporation) and eluted as ^{18}F$^-$/(Kryptofix 2.2.2)/K$^+$ complex. Initial radioactivity used in the labeling experiments at the start of synthesis ranged typically from 0.5 to 1.0 GBq. The complex was dried azeotropically at +120 °C with argon flow (45 mL min^{-1}) on a semiautomated synthesis unit (DM Automation), cooled to room temperature and dissolved in the solvent under study. The solution was transferred to a vial containing 1 mg of the dry PSi microparticles and mixed with shaking. The vial was placed on the preheated reactor on the synthesis unit and heated for the desired time.

Particles were separated from the reaction mixture with filtration through a 0.1 μm hydrophilic PTFE membrane filter (Omnipore, Millipore Corporation) and washed with 2 mL of DMF and 8 mL of absolute ethanol (Altia Oyj). Particles were eluted from the filter with 2 mL of ethanol and 4 mL of 1× PBS (phosphate buffered saline), pH 7.41. The solution was mixed with shaking and incubated at room temperature for 20 min to

Table 2. Decay-Corrected RCY ($n = 1-3 \pm$ SD) of Selected ^{18}F-Labeling Reactions

particle	solvent	T (°C)	acetic acid (μL)	RCY (%)	total synthesis time[a] (min)
^{18}F-THCPSi	DMSO	100	20	54	
	CH_3CN	50	20	30	
	DMF	50	20	40 ± 15	
		100	20	80 ± 8	
		120	0	81 ± 2	55.9−61.3
		120	20	73 ± 10	
^{18}F-TOPSi	DMSO	100	20	60	
	CH_3CN	50	20	34	
	DMF	50	20	35 ± 17	
		100	20	21 ± 4	
		120	0	55 ± 5	56.7−58.7
		120	20	37 ± 7	
^{18}F-TCPSi	DMSO	100	20	39	
	CH_3CN	50	20	31	
	DMF	50	20	39 ± 1	
		100	20	45 ± 7	
		120	0	79 ± 3	52.4−55.5
		120	20	48 ± 7	

[a] Total synthesis time from the end of bombardment (EOB) consists of elution and drying of the $K^+/(Kryptofix\ 2.2.2)/^{18}F^-$ complex (15 min), reaction (10 min), cooling (5 min), first filtration and elution (5 min), incubation in (1× PBS)−EtOH (20 min) and second filtration and elution (5 min). Times given in parentheses are approximate.

release free $^{18}F^-$ label from the pores of the microparticles. Particles were again collected by filtration on a 0.1 μm hydrophilic PTFE membrane, washed with ultrapure water and ethanol and released from the filter with 4 mL of ultrapure water. Radioactivity of both the filter and filtrate together with the residual activities retained on both after each step was measured with a dose calibrator (CRC-210, Capintec Inc.) and decay-corrected to the start of synthesis. For the biodistribution study ^{18}F-THCPSi microparticles were formulated into 1× PBS to a final concentration of 8.0−11.7 MBq mL^{-1}. Finally, a drop of the microparticle solution was applied to Whatman 1 chromatography paper (Millipore Corporation) and developed with ultrapure water for detection of residual free $^{18}F^-$ in the final particle product. Paper chromatographs were exposed to a digital imaging plate (Fujifilm TR2025) and scanned on a Fujifilm FLA-5100 scanner. The digital autoradiographs were analyzed on AIDA 2.0 imaging software (Raytest Isotopenmessgeräte GmbH).

2.3. In Vitro Label Stability Tests. The stability of the ^{18}F label was investigated with incubations in buffer solutions at three pH values, 2.33 (10 mM H_3PO_4), 7.41 (10 mM NaH_2PO_4) and 8.70 (10 mM Tris-HCl), in simulated gastric fluid (sGF, 2.0 g L^{-1} NaCl and 3.2 g L^{-1} porcine pepsin, pH 1.2), in fasted-state simulated intestinal fluid (FaSSIF, prepared according to ref 37) and in human plasma. Plasma was anonymous donor plasma from the Finnish Red Cross Blood Service (ethical permissions 55/2008 and 25/2011). Purified ^{18}F-labeled PSi microparticles were suspended in ultrapure water and divided into conical polypropylene tubes with the selected buffer or plasma (400 μL of particle solution to 4 mL of buffer or plasma) and mixed with shaking. Samples were incubated for 15, 30, 60, 120, 180, and 240 min. The pH stability tests were done at room temperature, whereas incubations in plasma and the simulated fluids were carried out at 36 ± 1.5 °C in a temperature-controlled water bath with continuous shaking at 200 rpm. Samples were mixed once more just prior to terminating the reaction by filtration of the particles out of the solution with a 0.45 μm hydrophilic mixed cellulose ester membrane (Millipore HA) and washing with 4 mL of the buffer under study or with 1× PBS in the case of the simulated fluid and plasma incubations. Both the filter and filtrate were measured on a dose calibrator to determine the fraction of radioactivity retained on the particles.

2.4. FTIR and XPS Spectroscopy. Free-standing PSi films and microparticles were labeled with carrier-added ^{18}F (0.172 mmol of potassium fluoride and 0.172 mmol of Kryptofix 2.2.2 added to the QMA eluate prior to the azeotropic distillation) using the above-mentioned protocol. Free-standing films were heated in a closed beaker in a temperature-controlled oil bath due to their larger size. Particles were purified as described above, but absolute ethanol was used instead of ultrapure water in the last step to release the particles. Particles were dried under an argon flow, and drying was continued under vacuum for two hours. The free-standing films were purified by sequential 10 min sonications in absolute ethanol, in ultrapure water and again in absolute ethanol (10 mL each) and allowed to dry at room temperature.

Transmission and attenuated total reflectance (ATR) FTIR spectra were obtained from the free-standing PSi films using PerkinElmer Spectrum BX spectrometer. The scan area was from 4000 to 550 cm^{-1} with a resolution of 4 cm^{-1}. The results are the average of 32 scans. The ATR accessory used was a single reflection MIRacleATR (Pike Technologies, Inc.) equipped with a diamond crystal. All the spectra are baseline corrected. The THCPSi spectra was obtained in transmission mode while the TCPSi and TOPSi spectra were obtained with the ATR-FTIR due to the high IR absorbance of the films below 1200 cm^{-1}.

The XPS measurements were carried out using PHI 5400 ESCA spectrometer (PerkinElmer Corporation) with a monochromated Mg Kα X-ray source ($h\nu$ = 1253.6 eV) using a 45° takeoff angle and 35.75 eV pass energy. The PSi microparticle samples were pressed on adhesive double-sided carbon tape before placement into vacuum under 10^{-8} mbar. The spectra were charge corrected by calibrating the binding energy of lattice silicon Si (2p) peak to 99.4 eV.

2.5. Biodistribution of ^{18}F-THCPSi Particles in the Rat GI Tract. All experimental procedures were approved by the National Committee for Animal Experimentation in Finland (State Provincial Office of Southern Finland, Hämeenlinna).^{18}F-THCPSi microparticles in 1× PBS, pH 7.41 were administered to two male Wistar rats (weighing 254 and 293 g, Laboratory Animal Centre, University of Helsinki, Finland) by intragastric gavage, and the animals were sacrificed at 2 and 4 h, respectively, after administration by CO_2 asphyxiation and cervical dislocation. Two control animals (248 and 272 g) were given free $^{18}F^-$ as ^{18}F-NaF in the vehicle. Animals were single-housed after administration with tap water and food (Global Diet 2016, Harlan Teklad) available ad libitum. The GI tract of the animals was excised and divided into segments based on anatomical identification for radioactivity measurements. The excised parts were stomach, duodenum, jejunum, ileum and ascending, transverse and descending colon. Sample from the skull was taken to measure ^{18}F accumulation in bone. Samples were weighed, and their radioactivity was counted on an automated gamma counter (Wizard 3, Perkin-Elmer) for 60 s.

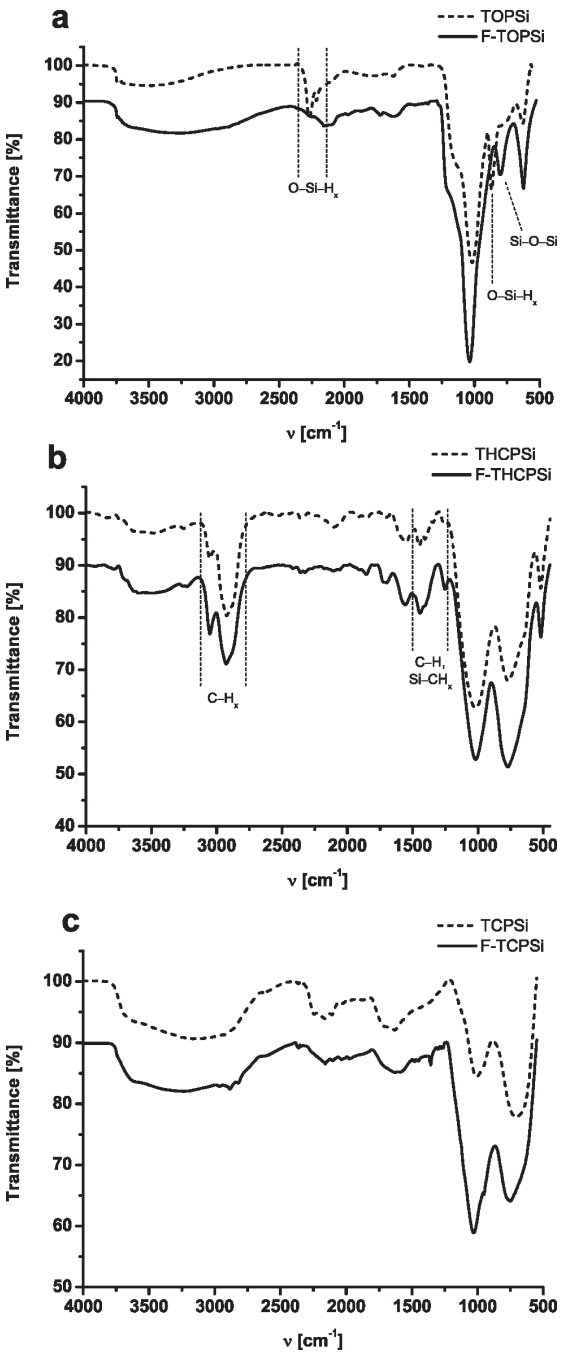

Figure 1. FTIR spectra of TOPSi (a), THCPSi (b) and TCPSi (c), before (dashed line) and after (solid line) carrier-added ^{18}F-radiolabeling. The spectra are baseline corrected and shifted vertically for clarity.

3. RESULTS AND DISCUSSION

3.1. ^{18}F-Radiolabeling of PSi Microparticles. ^{18}F-radiolabeling of PSi microparticles was carried out using activated nucleophilic ^{18}F-fluoride as $^{18}F^-/(Kryptofix\ 2.2.2)/K^+$ complex with acetic acid as an additive. The most successful reaction conditions investigated and the corresponding decay-corrected radiochemical yields (RCY) are given in Table 2. For THCPSi and TCPSi, the highest RCYs were obtained in DMF at temperatures above +100 °C. For TOPSi, DMSO yielded equally good results. Reactions in acetonitrile generally failed to give RCYs higher than 34%. Total synthesis times with particle purification typically ranged from 52 to 61 min, indicating that further surface modification of the ^{18}F-labeled particles would still be possible without compromising end product yield. Paper chromatography of the final ^{18}F-labeled PSi products confirmed that all the particle preparations were void of residual free $^{18}F^-$ at the end of radiosynthesis. Representative digital autoradiographs of the chromatography papers are given in Figure S1 in the Supporting Information.

Scheme 1. Plausible Sites for ^{18}F Incorporation on PSi Surfaces

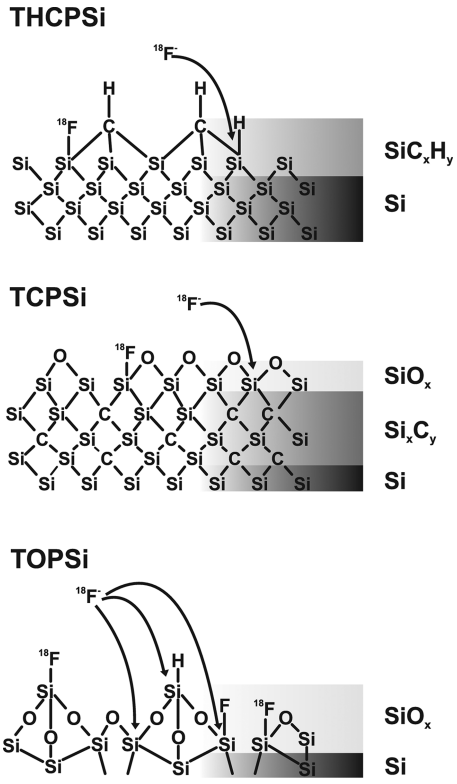

We found that the radiolabeling yield was not improved by the addition of acetic acid for any of the particle types studied, as has been suggested for the labeling of ^{18}F-fluorosilanes with hydrogen as a leaving group.[29] Radiolabeling yield for THCPSi was largely unaffected by the addition of acetic acid, whereas lower yields were observed for TOPSi and TCPSi, analogous to what has been reported previously for some sterically hindered silicon compounds.[30] The thermally oxidized surface of TOPSi is covered by Si−O−Si species which could serve as a good target for the nucleophilic attack of fluoride. Substitution of oxygen with fluoride should be promoted in acidic conditions that enhance the leaving group ability of oxygen. However, this was not observed in our study. Interestingly, XPS analysis of the TOPSi microparticles revealed relatively high initial fluorine content of the starting material (0.66 mass %). This fluorine may be carried over from the etching process and precarbonization treatment of the particles.[38] As isotopic exchange of silyl fluoride with $^{18}F^-$ can be achieved easily to a sterically hindered position even at room temperature,[32] it is possible that a Si−F to Si−^{18}F exchange takes place.

3.2. FTIR and XPS Characterization of ^{18}F-Labeled PSi Films and Microparticles. Due to high specific radioactivity of

$^{18}F^-$ conventional surface characterization methods are not sensitive enough to detect the newly formed Si−^{18}F bonds. Therefore, we radiolabeled free-standing PSi films and microparticles for FTIR and XPS studies, respectively, in the presence of added fluorine carrier (0.172 mmol of ^{19}F). Analysis of ^{18}F/^{19}F-THCPSi microparticles showed an expected increase in the XPS signal for fluorine (F 1s), from 0.39 to 1.15 mass % after carrier-added radiolabeling. For ^{18}F-TCPSi, the increase was only modest (from 0.36 to 0.42). Elemental analysis of the ^{18}F/^{19}F-labeled PSi microparticles is given in Table S1 in the Supporting Information. Both THCPSi and TCPSi particles are fabricated by acetylene treatment at 500 °C, and at this stage some residual hydrogen terminated silicon can still be seen in FTIR spectra. However, the further processing of TCPSi at 820 °C removes the remaining hydrogens from the surface, leaving a thin silicon oxide layer on top of the Si−C_x structure. The subtle increase in fluorine content after carrier-added labeling may be due to saturation of the possible fluorination sites, because in the carrier added conditions over 30000-fold excess of fluoride was used in contrast to the tracer conditions. Because of the high initial fluorine content of TOPSi particles, we were not able to see a detectable increase in the fluorine signal after the carrier-added labeling in the XPS analysis. Furthermore, if the primary mechanism for labeling the particles is via the proposed isotopic exchange of the residual silyl fluorides to $^{18}F^-$ on the surface, we would not expect to observe any increase in the fluorine content after radiolabeling.

The FTIR spectra obtained from THCPSi and TCPSi free-standing films both indicate negligible changes in the structure after the carrier-added labeling, as depicted in Figure 1. Obviously in order to successfully use the ^{18}F-labeled microparticles as a tracer for unlabeled PSi, one expects not to find detectable changes in the physicochemical properties of the material after radiolabeling, as illustrated here with FTIR spectroscopy. The CH_x stretching vibrations around 2900 cm^{-1} and the vibrations of various alkyl structures between 1200 and 1500 cm^{-1} characteristic for THCPSi remain unchanged after the labeling. Similar results are obtained with TCPSi, where little change occurs after the labeling. The appearance of small peaks in labeled TCPSi related to CH_x stretching can be assigned as residual DMF from the labeling process. In TOPSi films (Figure 1), the back-bond oxidized O_xSi-H_x stretching bands between 2150 cm^{-1} and 2300 cm^{-1} and the corresponding deformation modes at 870 cm^{-1} disappear after the labeling and features related to oxidation are emphasized, suggesting that the labeling strategy is not optimal for TOPSi. This can be observed from the strengthening of the symmetric Si−O−Si stretching vibrations at 800 cm^{-1}, and it is also detectable from the XPS signal for Si (2p) as an increase in the intensity of Si−O peak related to the Si−Si peak. Similar but minor oxidation can be observed from the Si (2p) signals of both TCPSi and THCPSi after labeling (Figure S2 in the Supporting Information). This may indicate that, during the radiolabeling, the immediate surface layers are oxidized and subsequently exposed to fluorine substitution. Detailed analysis of the XPS spectra is given in the Supporting Information. Possible Si−F vibrations in the FTIR spectra are difficult to detect in any of the labeled PSi films, as the characteristic peaks reside at lower wavenumbers. Also the far stronger silicon oxide related features in the spectra mask the possible stretching vibrations of Si−F_x at 972 cm^{-1}. Furthermore, storage in ambient conditions may eventually have hydrolyzed the formed Si−F structures, leaving the Si−O−Si structures behind.

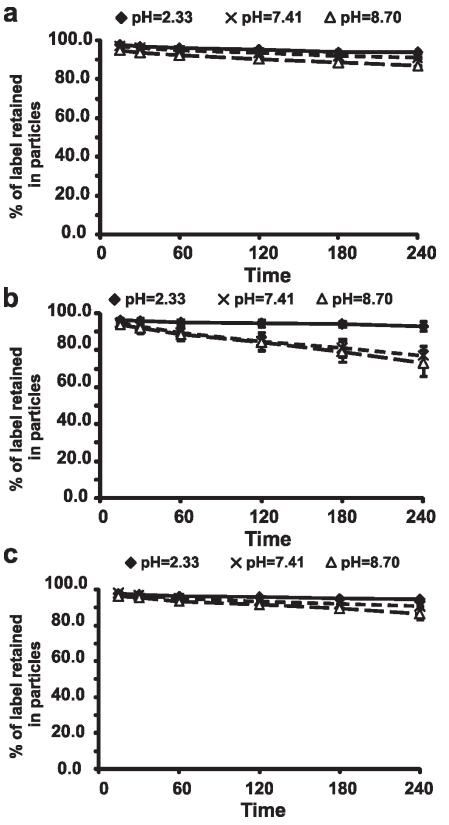

Figure 2. ^{18}F-label stability at different pH values for (a) ^{18}F-THCPSi, (b) ^{18}F-TOPSi, and (c) ^{18}F-TCPSi. Markers denote mean ± SD (n = 2).

Based on these findings we postulate that the ^{18}F binding to modified PSi surfaces can proceed depending on the material either by substitution for silyl hydrogens, by nucleophilic attack to Si−O−Si bridges or by isotopic exchange to residual silyl fluoride. Plausible sites for ^{18}F attachment to THCPSi, TCPSi and TOPSi surfaces are summarized in Scheme 1.

3.3. Radiolabel Stability. The hydrolytic stability of the synthesized Si−^{18}F bonds under physiological conditions has been shown to be impacted strongly by the substituents to the Si atom bearing the radioisotope.[28,30] Steric hindrance shielding the Si atom has been found to be especially important for stability of the bond. For example, the presence of bulky *tert*-butyl and aryl groups adjacent to the Si atom bearing the ^{18}F-label results in increased label stability toward hydrolysis and decreased cleavage rate of the label in vivo. Label instability is a key issue in the design of radiopharmaceuticals as the radiolabeled tracer and free radiolabel cannot be distinguished from one another once the image is obtained. Released $^{18}F^-$ accumulates in the bone increasing radiation burden to the subject and possibly interfering with the imaging in cases where the region of interest is located in close proximity of bone, such as in the central nervous system.

Here, label stability was investigated at three physiologically relevant pH values (2.33, 7.41 and 8.70) and in simulated gastric and intestinal fluids and in human plasma at +37 °C. The stability curves are given in Figures 2 and 3. ^{18}F-THCPSi and ^{18}F-TCPSi demonstrated excellent (>90% of ^{18}F bound to particles) stability of the radiolabel in all the pH values studied for up to four hours. Furthermore, all the particle types exhibited very high

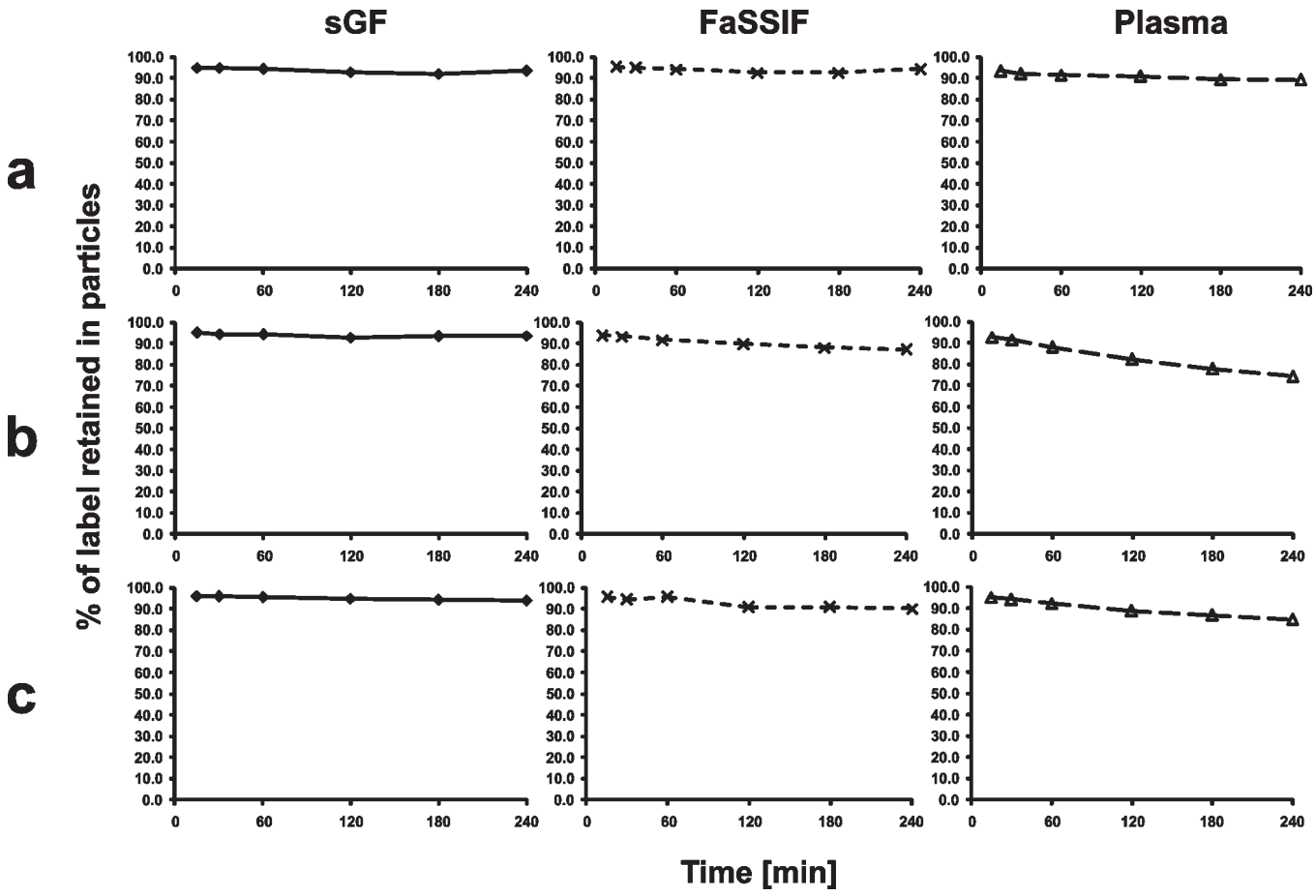

Figure 3. ^{18}F-label stability in simulated gastric (sGF) and fasted-state intestinal fluids (FaSSIF), and in human plasma at +37 °C: (a) ^{18}F-THCPSi, (b) ^{18}F-TOPSi, and (c) ^{18}F-TCPSi (n = 1).

label stability in biophysically relevant fluids sGF and FaSSIF, indicating that they could be used to study particle biodistribution in vivo after oral administration within the 6 to 8 h time frame allowed for by the half-life of ^{18}F. Both ^{18}F-THCPSi and ^{18}F-TCPSi also demonstrated sufficiently high label plasma stability for systemic administration. On the contrary, the stability of thermally oxidized ^{18}F-TOPSi is reduced at pH values above 7.41 and the instability is augmented in plasma under the experimental conditions studied. The hydrolytic instability of the radiolabeled TOPSi can be accounted for by the high hydrophilicity of the material, which allows OH^- ions to penetrate closer to the particle surface and hydrolyze the Si—^{18}F bond. In addition, the surface of TOPSi is relatively unstable at basic conditions (pH 8.70), and label is released due to dissolution of the particles over time. Nevertheless, as the duodenal pH will reside closer to neutral pH (as in FaSSIF) by the mixing of acidic stomach contents with duodenal fluid, oral administration of ^{18}F-TOPSi is also feasible. However, the observed fast decline in plasma stability over time indicates otherwise poorer in vivo imaging characteristics for this particle type.

3.4. Biodistribution of ^{18}F-THCPSi Microparticles in the Rat Gastrointestinal Tract. In order to evaluate the stability of the label and biodistribution of ^{18}F-labeled PSi microparticles in the GI tract after oral administration, ^{18}F-THCPSi microparticles were forwarded to a biodistribution study in rats. For simulation of the in vivo distribution of detached radiolabel, the biodistribution of free $^{18}F^-$ in the rat gastrointestinal tract was assessed with oral administration of ^{18}F-NaF in the vehicle. The passage of orally administered ^{18}F-THCPSi microparticles in the rat GI tract was markedly slower than the passage of ^{18}F-NaF in control animals (Figure 4). At the two-hour time point the bulk of the radioactivity for the particle-dosed animal resided in the stomach, whereas in the control it had reached the ileum, the most distal part of the small intestine. Four hours after administration, the particles had migrated to the ileum. By then free $^{18}F^-$ had reached the descending colon in the control animal. Additionally, significantly higher absorption of $^{18}F^-$ from the GI tract and subsequent uptake in bone was seen in control animals (Figure 5), whereas the accumulation of $^{18}F^-$ released from ^{18}F-THCPSi microparticles to bone was only on the order of 0.5% ID/g. Although the observed high stability might be deleterious in terms of THCPSi particle biodegradability after systemic administration, it could serve as a unique approach to oral drug delivery by an inert vehicle that is excreted after payload release. Our previous studies have demonstrated that THCPSi particles are strongly associated with Caco-2 cell monolayers (a cell culture model for the study of intestinal permeability), but extensive permeation of the particles across the monolayer was not observed, rendering the concept of payload release without particle permeation feasible.[22] Furthermore, the high stability of THCPSi particles is certainly an advantage with respect to the possibility of accommodating a wide array of both sensitive and reactive payloads.

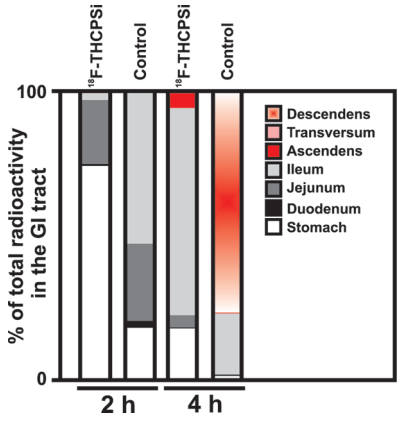

Figure 4. Distribution of radioactivity in the GI tract of rats dosed orally with ^{18}F-labeled THCPSi microparticles 2 and 4 h after administration, from left to right respectively. Control animals received free $^{18}F^-$ in the vehicle.

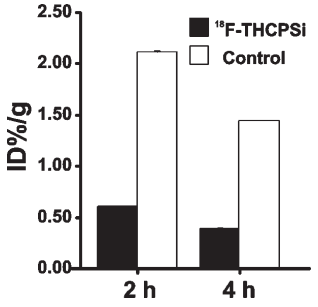

Figure 5. Distribution of radioactivity in the bone of rats dosed orally with ^{18}F-labeled THCPSi microparticles 2 and 4 h after administration. Control animals received free $^{18}F^-$ in the vehicle.

4. CONCLUSION

In conclusion, we have successfully labeled PSi microparticles with ^{18}F for the investigation of their biodistribution and performance as oral drug delivery carriers in vivo. For all particle types studied, direct nucleophilic fluorination with ^{18}F was achieved, but the yield of the radiolabeling was impacted by the initial surface modifications of the materials. Highest decay-corrected radiochemical yields were obtained in anhydrous dimethyl formamide at +120 °C. In these conditions, the radiolabeling proceeds likely by direct substitution of Si−^{18}F for residual Si−H groups or for oxygen in Si−O−Si structures on the modified porous silicon surface. The ^{18}F-labeled thermally hydrocarbonized and thermally carbonized microparticles exhibited high hydrolytic stability at physiological pH range and excellent stability in simulated gastric and intestinal fluids and in human plasma, confirming that they could be used to track microparticle biodistribution after both oral and intravenous administration. The biodistribution study with orally administered ^{18}F-THCPSi microparticles highlighted the utility of using an ^{18}F-radiolabel to investigate PSi particle passage in the GI tract over time and corroborated the observed in vitro radiolabel stability in vivo. The results demonstrate that ^{18}F-labeled PSi are suitable probes for the investigation of PSi biodistribution, encouraging further studies on their in vivo behavior with PET.

■ ASSOCIATED CONTENT

Supporting Information. Elemental analysis and XPS spectra of the carrier-added ^{18}F-labeled PSi materials with further discussion. Digital autoradiography for determination of free $^{18}F^-$ content in ^{18}F-labeled PSi. This material is available free of charge via the Internet at http://pubs.acs.org.

■ AUTHOR INFORMATION

Corresponding Author

*University of Helsinki, Laboratory of Radiochemistry, Department of Chemistry, P.O. Box 55 (A. I. Virtasen aukio 1), FI-00014 University of Helsinki, Finland. E-mail: mirkka.sarparanta@helsinki.fi. Tel: +358-9-19150134. Fax: +358-9-19150121.

■ ACKNOWLEDGMENT

Dr. Kerttuli Helariutta and Dr. Markus Nyman are thanked for production of the ^{18}F isotope. Luis Bimbo and Markku Heinonen are acknowledged for assistance in the preparation of the simulated fluids and the XPS measurements, respectively. Financial support from the Academy of Finland (decision numbers 127099, 123037, 122314 and 140965), the Jenny and Antti Wihuri Foundation, the Drug Discovery Graduate School and the University of Helsinki Research Funds is acknowledged.

■ REFERENCES

(1) Rudin, M.; Weissleder, R. Molecular Imaging in Drug Discovery and Development. *Nat. Rev. Drug Discovery* **2003**, *2*, 123–131.

(2) Jarzyna, P. A.; Gianella, A.; Skajaa, T.; Knudsen, G.; Deddens, L. H.; Cormode, D. P.; Fayad, Z. A.; Mulder, W. J. M. Multifunctional Imaging Nanoprobes. *Wiley Interdiscip. Rev.: Nanomed. Nanobiotechnol.* **2010**, *2*, 138–150.

(3) Salonen, J.; Laitinen, L.; Kaukonen, A. M.; Tuura, J.; Björkqvist, M.; Heikkilä, T.; Vähä-Heikkilä, K.; Hirvonen, J.; Lehto, V.-P. Mesoporous Silicon Microparticles for Oral Drug Delivery: Loading and Release of Five Model Drugs. *J. Controlled Release* **2005**, *108*, 362–374.

(4) Salonen, J.; Kaukonen, A. M.; Hirvonen, J.; Lehto, V. Mesoporous Silicon in Drug Delivery Applications. *J. Pharm. Sci.* **2008**, *97*, 632–653.

(5) Limnell, T.; Riikonen, J.; Salonen, J.; Kaukonen, A. M.; Laitinen, L.; Hirvonen, J.; Lehto, V.-P. Surface Chemistry and Pore Size Affect Carrier Properties of Mesoporous Silicon Microparticles. *Int. J. Pharm.* **2007**, *343*, 141.

(6) Wu, E. C.; Park, J.; Park, J.; Segal, E.; Cunin, F.; Sailor, M. J. Oxidation-Triggered Release of Fluorescent Molecules or Drugs from Mesoporous Si Microparticles. *ACS Nano* **2008**, *2*, 2401–2409.

(7) Wang, F.; Hui, H.; Barnes, T. J.; Barnett, C.; Prestidge, C. A. Oxidized Mesoporous Silicon Microparticles for Improved Oral Delivery of Poorly Soluble Drugs. *Mol. Pharmaceutics* **2010**, *7*, 227–236.

(8) Bimbo, L. M.; Mäkilä, E.; Laaksonen, T.; Lehto, V.; Salonen, J.; Hirvonen, J.; Santos, H. A. Drug Permeation Across Intestinal Epithelial Cells Using Porous Silicon Nanoparticles. *Biomaterials* **2011**, *32*, 2625–2633.

(9) Tasciotti, E.; Liu, X.; Bhavane, R.; Plant, K.; Leonard, A. D.; Price, B. K.; Cheng, M. M.; Decuzzi, P.; Tour, J. M.; Robertson, F.; Ferrari, M. Mesoporous Silicon Particles as a Multistage Delivery System for Imaging and Therapeutic Applications. *Nat. Nanotechnol.* **2008**, *3*, 151–157.

(10) Gu, L.; Park, J.-H.; Duong, K. H.; Ruoslahti, E.; Sailor, M. J. Magnetic Luminescent Porous Silicon Microparticles for Localized Delivery of Molecular Drug Payloads. *Small* **2010**, *6*, 2546–2552.

(11) Kilpeläinen, M.; Riikonen, J.; Vlasova, M. A.; Huotari, A.; Lehto, V. P.; Salonen, J.; Herzig, K. H.; Järvinen, K. In Vivo Delivery

of a Peptide, Ghrelin Antagonist, with Mesoporous Silicon Microparticles. *J. Controlled Release* **2009**, *137*, 166–170.

(12) Tanaka, T.; Mangala, L. S.; Vivas-Mejia, P. E.; Nieves-Alicea, R.; Mann, A. P.; Mora, E.; Han, H.; Shahzad, M. M. K.; Liu, X.; Bhavane, R.; Gu, J.; Fakhoury, J. R.; Chiappini, C.; Lu, C.; Matsuo, K.; Godin, B.; Stone, R. L.; Nick, A. M.; Lopez-Berestein, G.; Sood, A. K.; Ferrari, M. Sustained Small Interfering RNA Delivery by Mesoporous Silicon Particles. *Cancer Res.* **2010**, *70*, 3687–3696.

(13) Park, J.-H.; Gu, L.; von Maltzahn, G.; Ruoslahti, E.; Bhatia, S. N.; Sailor, M. J. Biodegradable Luminescent Porous Silicon Nanoparticles for In Vivo Applications. *Nat. Mater.* **2009**, *8*, 331–336.

(14) Anglin, E. J.; Cheng, L.; Freeman, W. R.; Sailor, M. J. Porous Silicon in Drug Delivery Devices and Materials. *Adv. Drug Delivery Rev.* **2008**, *60*, 1266–1277.

(15) Prestidge, C. A.; Barnes, T. J.; Lau, C.; Barnett, C.; Loni, A.; Canham, L. Mesoporous Silicon: a Platform for the Delivery of Therapeutics. *Expert Opin. Drug Deliv.* **2007**, *4*, 101–110.

(16) Chiappini, C.; Tasciotti, E.; Fakhoury, J. R.; Fine, D.; Pullan, L.; Wang, Y.; Fu, L.; Liu, X.; Ferrari, M. Tailored Porous Silicon Microparticles: Fabrication and Properties. *ChemPhysChem* **2010**, *11*, 1029–1035.

(17) Canham, L. T. Bioactive Silicon Structure Fabrication through Nanoetching Techniques. *Adv. Mater.* **1995**, *7*, 1033–1037.

(18) Low, S. P.; Voelcker, N. H.; Canham, L. T.; Williams, K. A. The Biocompatibility of Porous Silicon in Tissues of the Eye. *Biomaterials* **2009**, *30*, 2873.

(19) Kashanian, S.; Harding, F.; Irani, Y.; Klebe, S.; Marshall, K.; Loni, A.; Canham, L.; Fan, D.; Williams, K. A.; Voelcker, N. H.; Coffer, J. L. Evaluation of Mesoporous Silicon/Polycaprolactone Composites as Ophthalmic Implants. *Acta Biomater.* **2010**, *6*, 3566–3572.

(20) Godin, B.; Gu, J.; Serda, R. E.; Bhavane, R.; Tasciotti, E.; Chiappini, C.; Liu, X.; Tanaka, T.; Decuzzi, P.; Ferrari, M. Tailoring the Degradation Kinetics of Mesoporous Silicon Structures through PEGylation. *J. Biomed. Mater. Res., Part A* **2010**, *94A*, 1236–1243.

(21) Canham, L. T.; Reeves, C. L.; Newey, J. P.; Houlton, M. R.; Cox, T. I.; Buriak, J. M.; Stewart, M. P. Derivatized Mesoporous Silicon with Dramatically Improved Stability in Simulated Human Blood Plasma. *Adv. Mater.* **1999**, *11*, 1505–1507.

(22) Bimbo, L. M.; Sarparanta, M.; Santos, H. A.; Airaksinen, A. J.; Mäkilä, E.; Laaksonen, T.; Peltonen, L.; Lehto, V.; Hirvonen, J.; Salonen, J. Biocompatibility of Thermally Hydrocarbonized Porous Silicon Nanoparticles and their Biodistribution in Rats. *ACS Nano* **2010**, *4*, 3023–3032.

(23) Santos, H. A.; Riikonen, J.; Salonen, J.; Mäkilä, E.; Heikkilä, T.; Laaksonen, T.; Peltonen, L.; Lehto, V.; Hirvonen, J. In Vitro Cytotoxicity of Porous Silicon Microparticles: Effect of the Particle Concentration, Surface Chemistry and Size. *Acta Biomater.* **2010**, *6*, 2721–2731.

(24) Sailor, M. J.; Wu, E. C. Photoluminescence-Based Sensing With Porous Silicon Films, Microparticles, and Nanoparticles. *Adv. Funct. Mater.* **2009**, *19*, 3195–3208.

(25) Tasciotti, E.; Godin, B.; Martinez, J. O.; Chiappini, C.; Bhavane, R.; Liu, X.; Ferrari, M. Near-Infrared Imaging Method for the In Vivo Assessment of the Biodistribution of Nanoporous Silicon Particles. *Mol. Imaging* **2011**, *10*, 56–68.

(26) Serda, R. E.; Gu, J.; Bhavane, R. C.; Liu, X.; Chiappini, C.; Decuzzi, P.; Ferrari, M. The Association of Silicon Microparticles with Endothelial Cells in Drug Delivery to the Vasculature. *Biomaterials* **2009**, *30*, 2440–2448.

(27) Cai, L.; Lu, S.; Pike, V. W. Chemistry with [^{18}F]Fluoride Ion. *Eur. J. Org. Chem.* **2008**, *2008*, 2853–2873.

(28) Mu, L.; Höhne, A.; Schubiger, P.; Ametamey, S.; Graham, K.; Cyr, J.; Dinkelborg, L.; Stellfeld, T.; Srinivasan, A.; Voigtmann, U.; Klar, U. Silicon-Based Building Blocks for One-Step ^{18}F-Radiolabeling of Peptides for PET Imaging. *Angew. Chem., Int. Ed.* **2008**, *47*, 4922–4925.

(29) Höhne, A.; Yu, L.; Mu, L.; Reiher, M.; Voigtmann, U.; Klar, U.; Graham, K.; Schubiger, P.; Ametamey, S. Organofluorosilanes as Model Compounds for ^{18}F-Labeled Silicon-Based PET Tracers and their Hydrolytic Stability: Experimental Data and Theoretical Calculations (PET=Positron Emission Tomography). *Chem.—Eur. J.* **2009**, *15*, 3736–3743.

(30) Höhne, A.; Mu, L.; Honer, M.; Schubiger, P. A.; Ametamey, S. M.; Graham, K.; Stellfeld, T.; Borkowski, S.; Berndorff, D.; Klar, U.; Voigtmann, U.; Cyr, J. E.; Friebe, M.; Dinkelborg, L.; Srinivasan, A. Synthesis, ^{18}F-Labeling, and in Vitro and in Vivo Studies of Bombesin Peptides Modified with Silicon-Based Building Blocks. *Bioconjugate Chem.* **2008**, *19*, 1871–1879.

(31) Iovkova, L.; Wängler, B.; Schirrmacher, E.; Schirrmacher, R.; Quandt, G.; Boening, G.; Schürmann, M.; Jurkschat, K. *para*-Functionalized Aryl-di-*tert*-butylfluorosilanes as Potential Labeling Synthons for ^{18}F Radiopharmaceuticals. *Chem.—Eur. J.* **2009**, *15*, 2140–2147.

(32) Schirrmacher, R.; Bradtmöller, G.; Schirrmacher, E.; Thews, O.; Tillmanns, J.; Siessmeier, T.; Buchholz, H. G.; Bartenstein, P.; Wängler, B.; Niemeyer, C. M.; Jurkschat, K. ^{18}F-Labeling of Peptides by means of an Organosilicon-Based Fluoride Acceptor. *Angew. Chem., Int. Ed.* **2006**, *45*, 6047–6050.

(33) Sun, Y.; Yu, M.; Liang, S.; Zhang, Y.; Li, C.; Mou, T.; Yang, W.; Zhang, X.; Li, B.; Huang, C.; Li, F. Fluorine-18 labeled Rare-earth Nanoparticles for Positron Emission Tomography (PET) Imaging of Sentinel Lymph Node. *Biomaterials* **2011**, *32*, 2999–3007.

(34) Zhou, J.; Yu, M.; Sun, Y.; Zhang, X.; Zhu, X.; Wu, Z.; Wu, D.; Li, F. Fluorine-18-labeled $Gd^{3+}/Yb^{3+}/Er^{3+}$ Co-doped $NaYF_4$ Nanophosphors for Multimodality PET/MR/UCL Imaging. *Biomaterials* **2011**, *32*, 1148–1156.

(35) Rojas, S.; Gispert, J. D.; Martín, R.; Abad, S.; Menchón, C.; Pareto, D.; Víctor, V. M.; Álvaro, M.; García, H.; Herance, J. R. Biodistribution of Amino-functionalized Diamond Nanoparticles. In Vivo Studies Based on ^{18}F Radionuclide Emission. *ACS Nano* **2011**, *5*, 5552–5559.

(36) Salonen, J.; Björkqvist, M.; Laine, E.; Niinistö, L. Stabilization of Porous Silicon Surface by Thermal Decomposition of Acetylene. *Appl. Surf. Sci.* **2004**, *225*, 389–394.

(37) Galia, E.; Nicolaides, E.; Hörter, D.; Löbenberg, R.; Reppas, C.; Dressman, J. B. Evaluation of Various Dissolution Media for Predicting In Vivo Performance of Class I and II Drugs. *Pharm. Res.* **1998**, *15*, 698–705.

(38) Kolasinski, K. W. Etching of Silicon in Fluoride Solutions. *Surf. Sci.* **2009**, *603*, 1904–1911.